Ultrastructure of the eukaryotic aminoacyl-tRNA synthetase complex derived from two dimensional averaging and classification of negatively stained electron microscopic images

Mona Trempe Norcum*

Biochemistry Department, University of Mississippi Medical Center, 2500 North State Street, Jackson, MS 39216-4505, USA

Received 8 February 1999; received in revised form 22 February 1999

Abstract Several aminoacyl-tRNA synthetases in higher eukaryotes are consistently isolated as a multi-enzyme complex for which little structural information is yet known. This study uses computational methods for analysis of electron microscopic images of the particle. A data set of almost 2000 negatively stained images was processed through reference-free alignment and multivariate statistical analysis. Interpretable structural information was evident in five eigenvectors. Hierarchical ascendant classification extracted clusters corresponding to distinct image orientations. The class averages are consistent with rotations around and orthogonal to a central particle axis and provide particle measurements: approximately 25 nm in height, 30 nm at the widest point and 23 nm thick. The results also provide objective evidence in support of the working structural model and demonstrate the feasibility of obtaining the three dimensional structure of the multisynthetase complex by single particle reconstruction methods.

Key words: Aminoacyl-tRNA synthetase; Multisynthetase complex; Electron microscopy; Image analysis

1. Introduction

There is now strong evidence that complicated biological processes, such as protein biosynthesis, are highly organized in vivo. However, most details of the molecular interactions involved are unknown. Within this context, a subset of the eukaryotic aminoacyl-tRNA synthetases, the enzymes that covalently link amino acids with the proper tRNAs, are consistently isolated as a multiprotein complex. This multisynthetase particle is a highly intriguing, but little understood, characteristic of this family of enzymes. Knowledge of the structural details of the multisynthetase complex is necessary not only for a complete understanding of the mechanism of eukaryotic protein biosynthesis, but also underlies the elucidation of the principles of intracellular organization. Moreover, because the existence of a multisynthetase complex appears to be restricted to multicellular eukaryotes, an understanding of its structure and function may be of use as the targeted design of new anti-microbials turns to the aminoacyl-tRNA synthetases (reviewed in [1]). In addition, it is well known that auto-antibodies to these proteins are closely associated with inflammatory muscle diseases (reviewed in [2]) and so elucidation of the normal organization of these enzymes is a prerequisite to full understanding of the origination of this pathological immune response.

*Corresponding author. Fax: (1) (601) 984-1501.
E-mail: mnorcum@biochem.umsmed.edu

As isolated from a variety of eukaryotes ranging from mammals to insects (reviewed in [3,4]), the commonly isolated multi-enzyme complex contains nine aminoacyl-tRNA synthetase activities (Fig. 1A). These are the enzymes for arginine (dimer of 70 kDa polypeptides), aspartic acid (dimer of 56 kDa polypeptides), glutamine (95 kDa), isoleucine (140 kDa), leucine (132 kDa), lysine (dimer of 77 kDa polypeptides) and methionine (105 kDa), as well as the bifunctional synthetase for proline and glutamic acid (160 kDa). Three additional proteins which are identified by their apparent masses (p43, p38, p18) are also part of the complex, but their stoichiometries and functions are not yet known with certainty. However, p43 may be a precursor to a cytokine [5] and p18 is likely to be involved in association of the multisynthetase complex with other components of the protein biosynthesis [6]. Overall, the mass of the multiprotein particle is approximately $1.1–1.2\times10^6$ Da. In negatively stained electron micrographs (Fig. 1B), the particle appears in several orientations including triangular, rectangular and square shapes [7,8].

A working structural model of the multisynthetase complex as a cup or elongated 'U' was proposed several years ago based on a subjective analysis of low resolution electron microscopic images [7]. More recently, evidence for the arrangement of the eight synthetase polypeptides within the multienzyme complex into three domains was presented based on reversible chemical crosslinking, coupled with earlier data such as dissociation experiments [8,9]. To refine and test these models, higher resolution structural details are needed.

This study presents the first application of computational microscopy to the multi-enzyme aminoacyl-tRNA synthetase complex. That is, a two dimensional analysis has been conducted of negatively stained images in order to test the suitability of the molecule for reconstruction of a high resolution three dimensional structure by single particle methods. The results obtained provide objective evidence in support of the working model, supply more precise particle measurements and set the stage for high resolution studies.

2. Materials and methods

The multisynthetase complex was isolated from rabbit reticulocyte lysate as previously described [9]. Discontinuous denaturing electrophoresis [10] was on a 7.5% acrylamide gel with bands visualized by alkaline silver stain [11]. For electron microscopy, samples at approximately 0.3 mg/ml in storage buffer (50 mM HEPES, pH 7.4, 1 mM dithiothreitol, 0.5 mM EDTA, 50% glycerol) were diluted with an equal volume of running buffer (25 mM HEPES, pH 7.2, 25 mM NaCl) and stabilized by the addition of glutaraldehyde to a final concentration of 0.3% [7]. The resulting 50 μl volume was chromatographed over a gel filtration HPLC column (GPC 300, Alltech) that was equilibrated in the running buffer and calibrated with a mixed gel filtration standard (Bio-Rad). Fractions eluting at approximately

PII: S0014-5793(99)00287-2

1×10^6 Da were then negatively stained with 1% uranyl acetate using a double carbon method [7,8]. Electron micrographs were obtained with a LEO 912AB microscope operating at 80 kV at an absolute magnification of 25 000 using the spectrometer slit to improve the contrast by removing inelastically scattered electrons.

Electron micrographs were digitized on a flatbed scanner at an optical resolution of 1200 dpi, which corresponds to 8.47 Å/pixel on the image scale. All subsequent image processing utilized the Spider (version 5.0) and Web programs [12] on a Silicon Graphics Indigo2 workstation. The data set consisted of 2083 images of the multisynthetase complex. Particle alignment used a reference-free algorithm incorporated in the apsr function which combines rotational and translational alignment. The procedure was self-limiting after three cycles, which resulted in a resolution limit for the global average of 39.5 Å as measured by fourier shell correlation of half data sets at a cut-off of 0.5. After selection of properly aligned images, the classification of 1956 images used principal component analysis over 10 factors followed by hierarchical ascendant clustering with complete linkage.

3. Results

3.1. The global average of images of the multisynthetase complex

Fig. 1 shows the average (C) of all aligned images in the data set. The overall shape is triangular with rounded edges. The only distinguishing features are the dark oval of dense stain at one edge and one high density spot in the upper right hand corner. The lack of interimage variance in these areas (D) indicates that these were the primary reference points found by the alignment algorithm. As seen by the white ring, the most variance is in the periphery of the average. This suggests that there are differences in particle orientations within the data set resulting in a variety of observed shapes. However, the overall density is rather even throughout the average (E), with the exception of the one spot mentioned above. Thus, there is no marked asymmetry in the particle mass distribution.

3.2. Multivariate statistical analysis of the image data set

In order to objectively sort out the expected image orientations, multivariate statistical analysis using a principal component algorithm was employed. This analysis expresses the image data as a set of multidimensional vectors. A covariance matrix is formed and then analyzed by the eigenvector method of ordination (reviewed in [13]). In this case, the factor space was delineated by 10 eigenvectors (or factors), each of which will contain different components of the interimage variation. A corresponding eigenvalue describes the relative amount of difference between the images explained by each factor. By ordering these percentages into a histogram, the factors which are the most important in representing the information within the data set are identified. The histogram for this data set (Fig. 2A) indicates that over 5% of the total interimage variance is contained in the first eigenvector or factor. However, not until factors 6 through 10 does the fall-off of the eigenvalue percentage become smooth, that is, approaching the

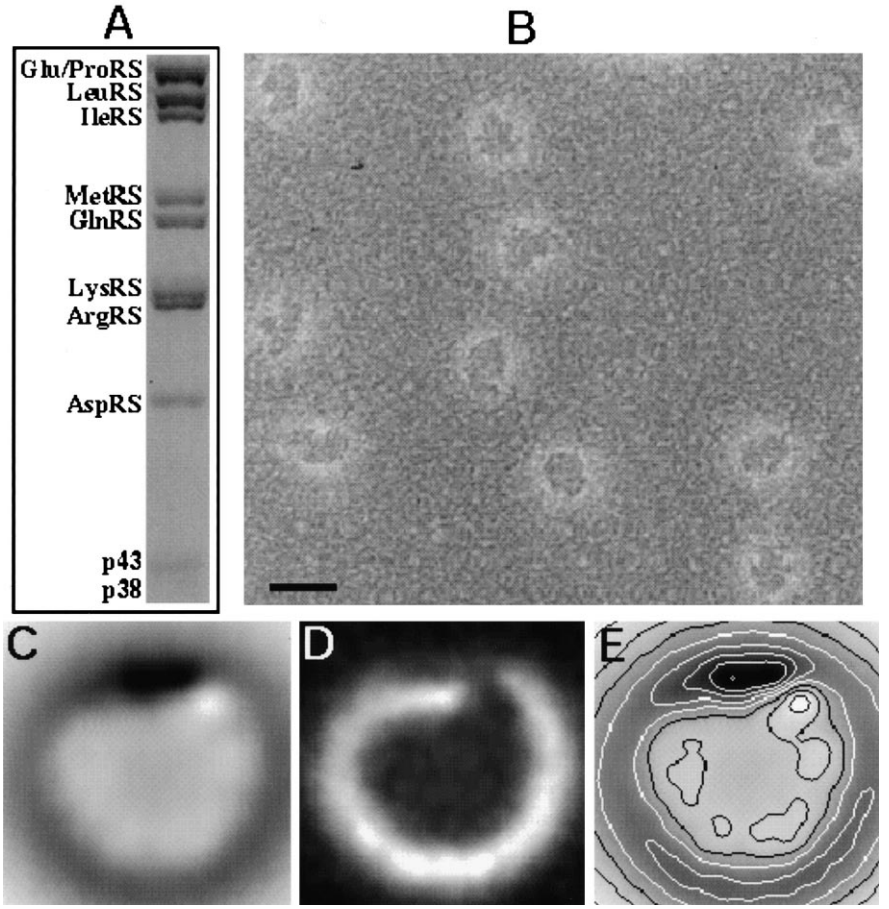

Fig. 1. Polypeptide pattern and electron microscopic views of the multisynthetase complex. A: SDS-polyacrylamide gel stained with silver. B: Representative electron micrograph of negatively stained particles. The scale marker measures 25 nm. C: Global average of data set after reference-free alignment. D: Variance of the average. E: Average with superimposed density contours.

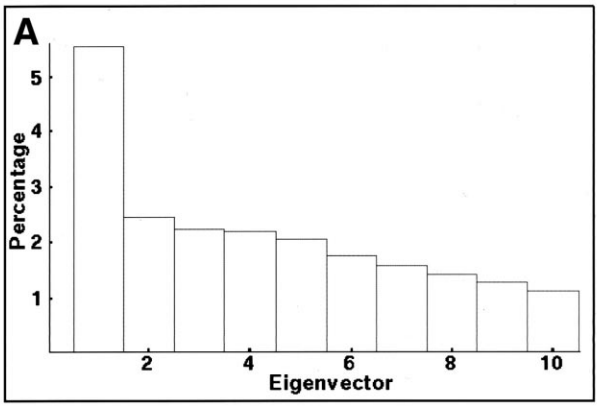

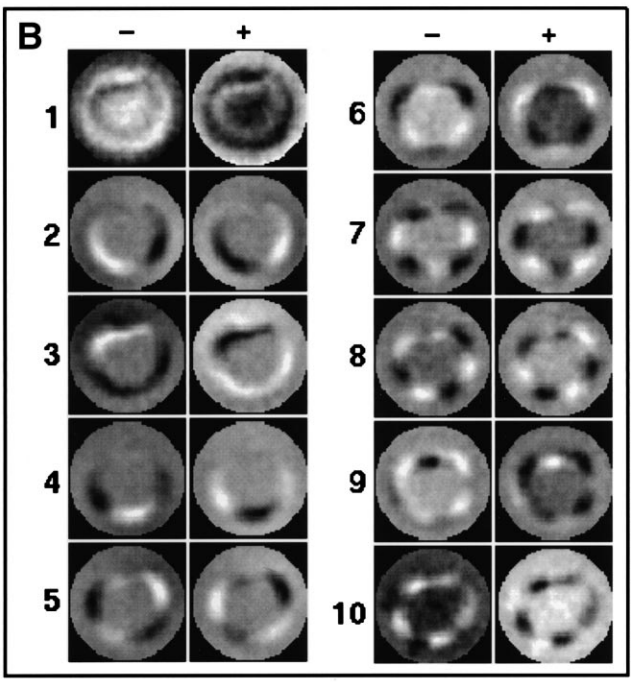

Fig. 2. Multivariate statisitical analysis of the data set using the principal component algorithm. A: Eigenvalue histogram over the 10 calculated vectors. B: Complementary pairs of importance images calculated at both extremes of each vector.

level of signal noise. This suggests that factors 2 through 5 are based on interpretable image information.

In order to visualize the structural variations within the images that separate the data along the various factors, it is helpful to calculate eigenimages or importance images [14]. These examine image elements at the negative and positive extremes of each vector and are generated as complementary pairs that highlight the image areas responsible for the pattern of image variation expressed by each factor. Such an analysis for this data set (Fig. 2B) shows that at least the first five are readily explained. Factor 1 corresponds to generalized changes in the stain density around and over the surface of the particles as demonstrated by the white ring around the particle and diffuse white areas over its surface at the negative end of the factor. Similarly, the complementary importance image at the positive end shows these areas as extremely dark. The white crescent at the lower left edge at the negative end of factor 2 shifts to the right side of the importance image at the positive end. This corresponds to a movement of density between the lower left edge and right side and suggests a change in 'handedness', or moving from one orientation to its mirror image. The third factor again shows a shift of mass from one edge of the particle to another, but this time moves from an arc at the upper left to a relatively diffuse distribution along the right and lower edges. This would convert the triangular shape into a square or rectangle. The change encompassed by factor 4 is the removal of mass at the lower edge and redistribution to both side edges. This would correspond to a change in image orientation from having its long axis vertical to horizontal. The eigenimages corresponding to the changes detected in factor 5 show a shift of two arcs of mass at opposing ends of the particle to the orthogonal orientations, that is,

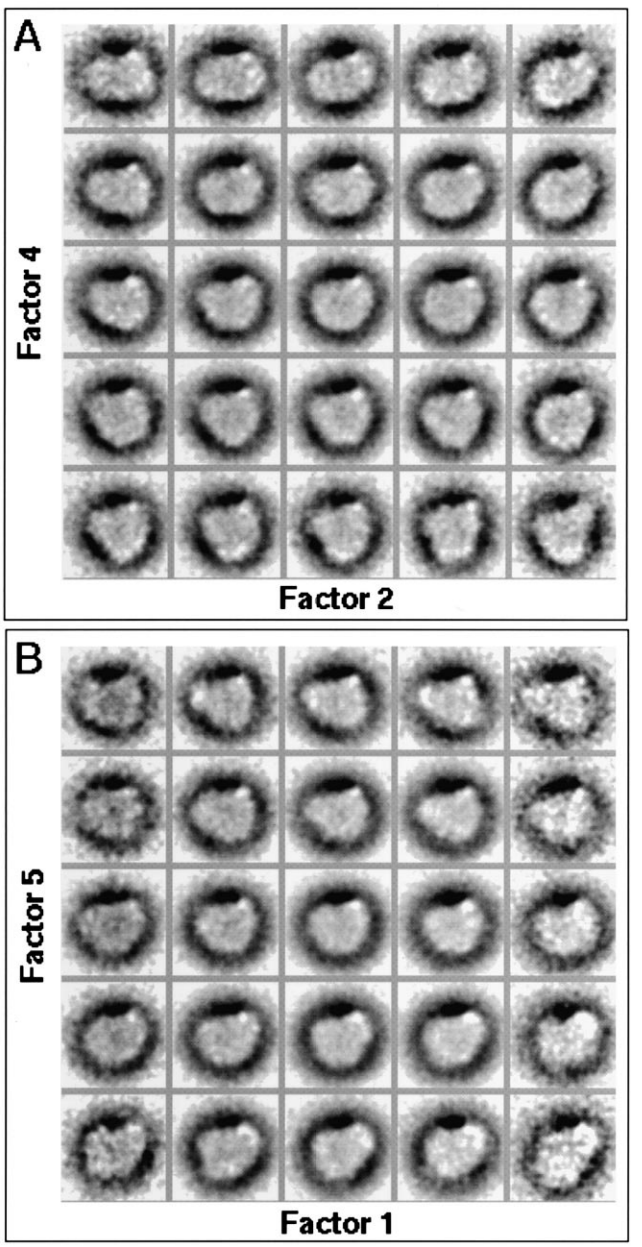

Fig. 3. Visible factor maps containing averages of images calculated over regular grid patterns covering the chosen factors. A: Factor 2 (handedness) versus factor 4 (shape change). B: Factor 1 (stain density) versus factor 5 (handedness).

one at the lower left and a larger density upper right to upper left and lower right, respectively. This would again result in changing the handedness of the particle or changing between mirror images.

Another method of visualizing the structural variations corresponding to the eigenvectors or factors is to calculate image averages along each. Fig. 3 shows two examples of factor maps, which demonstrate the validity of the interpretations based on importance images. A shows calculated image averages ordered according to factor 2 in the horizontal axis and factor 4 in the vertical axis. That factor 2 corresponds to a change in handedness is particularly clear in the bottom row. Moving from left to right, the image averages change from a triangular shape with the pointed end at the upper left to one where it is in the upper right. That is, the orientation of particle shape changes from left-handed to right-handed. From top to bottom of panel A, the particle shapes change from rectangular with the long axis oriented horizontally through an almost square shape to triangular views with a slightly longer vertical axis than horizontal. This confirms the above interpretation for the image variance tracked in factor 4. B contrasts factor 1 on the horizontal axis with factor 5 on the vertical axis. It is clear that as one considers factor 1 from the left side of the map to the right, the stain distribution changes from a relatively even peripheral ring to a primary concentration near the center of the top edge of the particle. Factor 5 is indeed similar to factor 2 in tracking changes in orientation. That is, moving from the top to the bottom of each column of the map, one can see that the orientation of each shape changes from left-handed to right-handed.

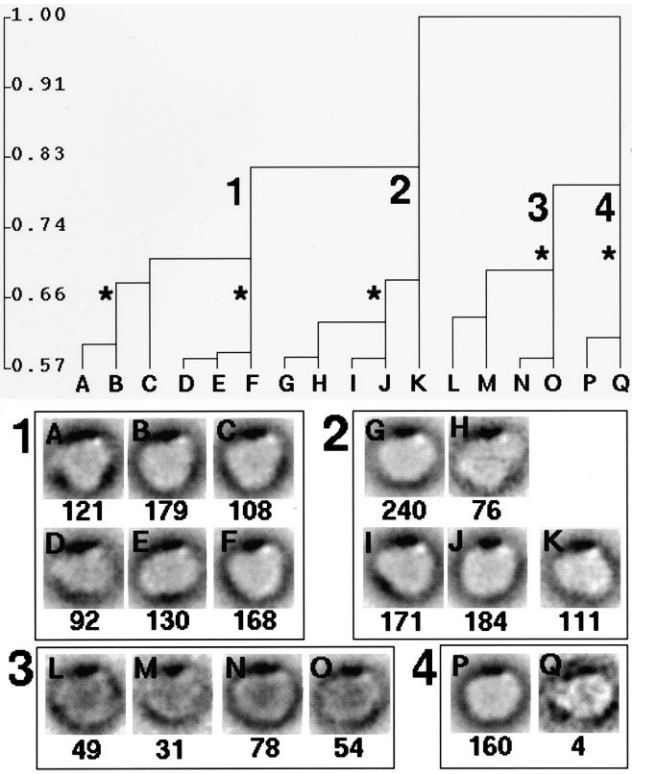

Fig. 4. Hierarchical ascendant classification of image clusters. The class averages of clusters are grouped according to the four major branches of the dendrogram. Letters relate each cluster average to its position in the dendrogram. The number of images within each cluster is given below each average.

3.3. Hierarchical ascendant classification of image clusters

The marked changes in shapes of the image averages that are visible in the factor maps indicate that the multivariate statistical analysis is detecting distinct particle orientations within the data set. Hierarchical ascendant classification organizes the image clusters incorporating all 10 of the vectors used in the principal component analysis. Fig. 4 shows the resulting rooted dendrogram truncated at a level of 17 classes. This truncation level was chosen to show distinct particle orientations while maintaining enough images in each class to provide meaningful averages. The classification tree initially splits into two major branches. One contains 80% (classes A through K) and the other 20% (classes L through Q) of the images. Subsequently, each of these splits relatively even in two. The image averages corresponding to the classes are presented in numbered groups corresponding to these four stable clusters.

Cluster 1 contains two arms each composed of three classes. Within the first arm, classes A and B are more related than class C. All are triangular, similar to the global average, but differ somewhat in shape. Class A shows an extra diffuse mass at the upper left corner, which likely reflects the occasional observations of particles with what appears to be either an extended 'tail' or more likely overlying debris. Classes B and C are both almost symmetrical triangles with rounded vertices and one slightly concave edge. As a way to correlate such averages with other orientations of the particle, they are termed the face view. Because these are projections, this also could depict the back view. Those averages with a more pointed end, such as class A, are interpreted as partial rotations of a particle and so are termed intermediate views. In the second arm of cluster 1, classes D and E are best characterized as rectangular and appear to represent further rotation around the long axis of the particle. Such views are termed side orientations. In contrast, class F is again an almost symmetric triangular shape. By comparison of their peripheral shapes, it appears that classes B and F are related by mirror symmetry.

Cluster 2 contains two arms with two closely related classes in each (G and H, I and J), as well as one independent group. Of the four classes in the first two arms, two are relatively square shapes (G and J, respectively). The other two are triangular with distinct long and short axes, as well as one more pointed vertex (I and H). The two triangular classes are related by mirror image symmetry and can be interpreted as additional rotation from the face into intermediate orientations. Classes G and J appear to have resulted from intermediate views that also are partially rotated in an orthogonal direction, that is, corresponding to partial tilts out of the plane of the support film. Class K also has elements of both types of rotations. These image classes are termed combination' orientations.

Cluster 3 is characterized by two arms, each containing two related classes. With the exception of class M, all of these averages are relatively square and have stain density in the centers of the particles. These are interpreted as top views orthogonal to the face or intermediate orientations. That is, the view of the particles is down into the center of the cup [7,8] from the open edge.

Cluster 4 contains one major image type (class P) and a few

outlier images (class Q). The main image class is almost square, similar to the views in cluster 3. However, this time the stain density is even throughout the molecule. This leads to the interpretation of these images as being of the bottom or closed end of the particle.

3.4. Major structural features

The major orientations seen in the averages of related clusters of images are presented in Fig. 5 (column A) along with the density contours within each average (column B). A schematic diagram (column C) is included in order to demonstrate the positional relationship of the types of particle views. The cluster averages were calculated at the positions of the classification scheme (Fig. 4) indicated by asterisks.

Row 1 shows the relatively symmetric face (or back) projection which is diagrammed as consisting of three domains arranged in a relatively symmetrical triangle. The particle in this orientation measures 33 nm at its widest point and approximately 27 nm along an axis drawn from one vertex to the midpoint of the other side of the image. The contour overlay indicates a higher density distribution near all three vertices than in the center of the particle, which is consistent with an interior channel. Classes B, C and F from the classification scheme (Fig. 4) represent this view and correspond to approximately 23% of the images in the data set. Row 2 depicts the intermediate view which is formed by partial rotation of the particle around the axis indicated in the scheme. This projection measures approximately 32 by 23 nm and brings the densities of two of the vertices into closer juxtaposition within the projection. Such image classes are A, D, H and I, which together contain another 23% of the images. Additional rotation around the axis would give the rectangular side view as seen in class E of Fig. 4. This orientation comprises only about 7% of the data set and so is relatively rare. It is an important projection because it gives an estimate of the thickness of the particle as approximately 23 nm.

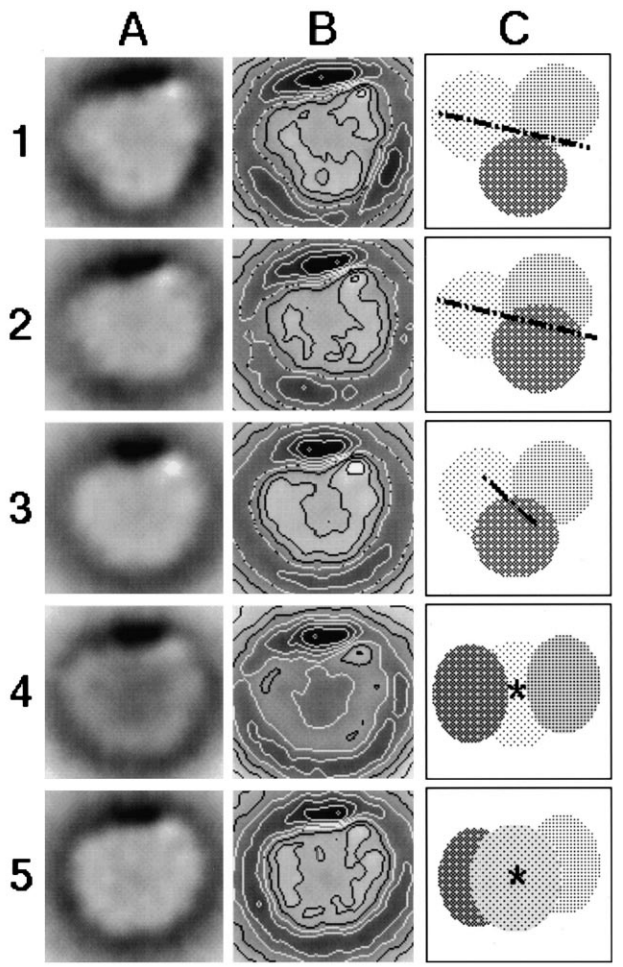

Fig. 5. Averaged images of the multisynthetase complex (A), density contour maps of each cluster average (B) and schematics (C) demonstrating the relationship of the characteristic particle orientations. Lines and asterisk indicate the rotational axis relating each view. Row 1: face, row 2: intermediate, row 3: combination, row 4: top, row 5: bottom.

An average containing combination views as well as intermediate views is given in row 3. This results in a structure of similar measurements to the average in row 2, but in shape is a hybrid of a square and a triangle with rather even density distribution throughout. These combination views result from intermediate axial rotations and partial tilting out of the plane. This type of projection is seen for about 30% of the data set (classes G, J and K). Rows 4 and 5 are the proposed end views. Each resembles a square, especially the latter which measures 30 by 24.5 nm. These result from orthogonal rotation out of the plane of the support film. The top and bottom views can be differentiated by either the presence (row 4) or absence (row 5) of visible central stain, respectively. Comparison of the two emphasizes the hole in the center of the top view, that is, a view down the interior channel, which is not seen in the view from the closed bottom edge. About 10% of the images are seen in each of these orientations.

4. Discussion

These averages and interpretations are consistent with the characteristic views defined by subjective analysis of negatively stained multisynthetase complex [7]. These were a cup or U shape, a triangle, a rectangle, a filled square and a square with a central hole. These can be directly correlated to the face, intermediate, side bottom and top views detected by mathematical analysis of the image data. Whether obtained subjectively or objectively, these views are consistent with various rotations relative to an overall particle shape as a somewhat pointed U. The more recent working model [9] incorporates information regarding the internal arrangement of the polypeptides into three domains, that is, the overall shape is composed of two arms and a base. The measurements obtained in this study provide additional evidence in support of the proposed shape of the structure. The length of the long axis of the face, intermediate and side views are all essentially the same. Thus, these likely represent a continuum of projections after rotation around a central particle axis. Moreover, measurements of the short axis of the side are similar to those of the top and bottom views. The model predicts that these should both correspond to the particle thickness. However, the long axis of the top and bottom views is approximately 10% smaller than the span of two vertices of the face view. This suggests that there is some inherent variability in the position of the arms of the multisynthetase complex or that some distortion occurs by flattening between carbon layers. It should be possible to distinguish between these possibilities, as well as to obtain additional structural details at

higher resolution, by using alternative techniques in sample preparation and imaging. For example, work is currently underway to label specific sites within the particle and to use cryo-electron microscopy techniques for viewing frozen hydrated samples.

Nonetheless, it is clear that even low resolution negatively stained images of the multisynthetase complex are rich in information regarding the ultrastructure of this multiprotein particle. Statistical analysis of the data set is able to extract distinct image classes. These classes are consistent with and provide additional support for the working model of the particle's structure. In addition, image averaging has provided new information. Not only are reliable particle measurements now known, but it is also clear that most of the image classes are slightly asymmetric and several are related by handedness or as mirror images. These data demonstrate that the particle is amenable to image reconstruction methods via single particle methods. Therefore, determination of a three dimensional structure of the multisynthetase complex should be straightforward. Such work is currently underway in this laboratory.

Acknowledgements: This work was supported in part by US Army Research Office Grants DAAH04-94-G-0335 and DAA04-95-1-0318. Mr Anthony Warrington is thanked for the excellent technical assistance with protein purification and HPLC analyses. Sincere gratitude is expressed to Dr Nicolas Boisset for a comprehensive introduction to image analysis.

References

[1] Schimmel, P., Tao, J. and Hill, J. (1998) FASEB J. 12, 1599–1609.
[2] Targoff, I.N. (1994) Rheum. Dis. Clin. North. Am. 20, 857–880.
[3] Kisselev, L.L. and Wolfson, A.D. (1994) Prog. Nucleic Acid Res. Mol. Biol. 48, 83–142.
[4] Yang, D.C.H. (1996) Curr. Top. Cell. Reg. 34, 101–136.
[5] Quevillon, S., Agou, F., Robinson, J.-C. and Mirande, M. (1997) J. Biol. Chem. 272, 32573–32579.
[6] Quevillon, S. and Mirande, M. (1996) FEBS Lett. 395, 63–67.
[7] Norcum, M.T. (1989) J. Biol. Chem. 264, 15043–15051.
[8] Norcum, M.T. (1991) J. Biol. Chem. 266, 15398–15405.
[9] Norcum, M.T. and Warrington, J.A. (1998) Prot. Sci. 7, 79–87.
[10] Laemmli, U.K. (1970) Nature 227, 680–685.
[11] Giulian, G.G., Moss, R.L. and Greaser, M. (1983) Anal. Biochem. 129, 277–287.
[12] Frank, J., Radermacher, M., Penczek, P., Zhu, J., Li, Y., Ladjadj, M. and Leith, A. (1996) J. Struct. Biol. 116, 190–199.
[13] Frank, J. (1990) Quart. Rev. Biophys. 23, 281–329.
[14] Frank, J. and van Heel, M. (1982) J. Mol. Biol. 161, 134–137.